Processing and Application of Ceramics 14 [1] (2020) 9–18
https://doi.org/10.2298/PAC2001009V

Study of barium titanate/nickel-zinc ferrite based composites: Electrical and magnetic properties and humidity sensitivity

Mirjana M. Vijatovic Petrovic[1,*], Adis Dzunuzovic[1], Jelena D. Bobic[1], Nikola Ilic[1], Ivan Stijepovic[2], Biljana D. Stojanovic[1]

[1]*Institute for Multidisciplinary Research, Belgrade University, Kneza Višeslava 1, Belgrade, Serbia*
[2]*Faculty of Technology, University of Novi Sad, Bulevar cara Lazara 1, Novi Sad, Serbia*

Received 21 August 2019; Received in revised form 10 December 2019; Accepted 20 January 2020

Abstract

Composites based on barium titanate and nickel zinc ferrite doped with cooper and samarium were prepared by a mixing method. The formation of barium titanate tetragonal crystal structure and nickel zinc ferrite cubic spinel structure was identified. Polygonal grains were formed in all three types of ceramics. Due to the very high conductivity of ferrite phase in the materials the ferroelectric hysteresis loops were roundish and not typical for classical ferroelectric material. The break down field was found to be similar for all compositions. Leakage current measurements have shown the existence of different types of conductivity mechanisms in each material. The impedance analysis suggested a bit stronger impact of grain boundaries on total conductivity of the composites and the mechanism of polaronic conduction of two types. The magnetization of the composites is lower than for the pure ferrite phase and corresponds to the weight fraction of the ferrite phase. The soft magnetic nature of these composites might be very useful for development of multifunctional devices which will be able to switch the magnetization with small external magnetic field. Humidity sensing properties of the prepared ceramics were also investigated.

Keywords: *composites, electrical properties, magnetic properties, humidity sensitivity*

I. Introduction

During the last couple of decades there is a growing interest in multiferroic materials (MF). Multiferroic materials are new class of materials that exhibit magnetoelectric effect as a combined effect of electrical and magnetic properties. They can be single phase, when one phase possesses both electrical and magnetic properties as well as ME effect, and multiphase (composite) which is consisted of phases with ferroelectric/ferroelastic properties and phases with ferromagnetism. Coupling of these properties in the composite material can induce magnetoelectric effect in the material which is "product proper" and exists only in MF composites when phases are homogeneously mixed together [1]. Singe phase multiferroics studied till now ($BiFeO_3$, $BiMnO_3$, $YMnO_3$ etc.) have shown weak magnetoelectric coupling and this problem could be solved by the preparation of composite MFs in which stronger coupling between electric and magnetic field via strain was noticed. Intensive research in this field has proven that it is not such a simple job, since individual properties of each phase are being diluted in the composites. Dielectric permittivity of the MFs is much lower in comparison with the pure dielectric phase and magnetic properties are proportional to the magnetic phase content in the MFs [2–6].

Lot of different compositions are being studied and developed during the years. As a good ferroelectric compounds, barium titanate based materials are usually used, as well as PZT and PMN as a materials with high piezoelectric coefficient. Ferromagnetic materials, such as different types of ferrites, $NiFe_2O_4$, $CoFe_2O_4$, $NiZnFe_2O_4$ etc. with high magnetostrictive coefficients were commonly used as a magnetic phase in the composite. Basically, it is necessary to have a mechanical coupling between the magnetostrictive phase and piezoelectric phase in the composites [7,8]. Also, it is very important to combine these properties by the optimization of processing parameters and adjusting the molar

*Corresponding author: tel: +381 11 2085 039,
e-mail: *miravijat@yahoo.com*

ratio between the phases in order to distinguish the highest ME output of the composite material. The nickel ferrite combines wide range of useful magnetic properties with relatively low electrical conductivity and high value of magnetization. In order to improve electrical and magnetic properties of this material, Jahn-Teller ions such as zinc, manganese or copper were commonly used as dopants. Doping with these ions, which have very high mechanical coupling, can enable higher magnetostriction and lower conductivity [9,10]. Nickel zinc copper ferrite was found to be very interesting soft magnetic material with spinel structure due to its low cost, high resistivity and low eddy current losses. It is conventionally used to improve densification as well as electromagnetic properties [11–13]. Literature data have shown that the addition of Cu in the nickel zinc ferrite causes also structural phase transition accompanied by changes in crystal symmetry (from cubic to tetragonal) [11,12]. Some earlier reports showed that the bulk density, electrical resistivity and initial permeability increased considerably with the copper concentration up to 20 at.%. Saturation magnetization and Curie temperature decreased with Cu addition [14]. Such a change of the nickel zinc ferrite doped with Cu makes this material suitable for use in high frequency applications and as data storage devices [12,14]. On the other hand, some studies showed that inclusion of samarium in nickel zinc ferrite inhibits grain growth and increases the density of the ceramics [15]. Usakova *et al.* [16] noticed that addition of Sm in the Cu-Zn-ferrite causes decrease of coercivity and by a careful addition of Sm, the magnetic properties of this material can be tailored.

Spinel-type materials are often used as a very promising resistive type humidity sensing materials due to its high resistivity and chemical stability. The electrical resistance decreases when material is placed in the humid atmosphere. Main sensing mechanism is based on the Grouthuus chain reaction [17]. At the same time, barium titanate was also proven to be very good material for humidity sensing [18,19]. Generally, when relative humidity (*RH*) is low, water molecules chemisorb on the grain surfaces due to the formation of chemical bond between active metal oxide surface and oxygen of the first water layer. This bond is not affected by the further change in humidity. Further layers of water molecules are physically adsorbed and they can dissociate under the high electric field effect. The charge transport occurs when the hydroxyl groups as a surface charge carriers release a proton to a neighbouring water molecule, which upon receiving it releases another proton and so on [20–22].

Based on previous arguments, in this study, composites containing spinel nickel-zinc ferrite doped with copper and samarium and ferroelectric barium titanate were prepared by mixing method. Modification of electrical and magnetic properties of composites in comparison with pure constituent phases was noticed and investigated in detail. Humidity sensitivity and stability of obtained materials were also analysed.

II. Experimental procedure

Pure barium titanate (BT) and nickel-zinc ferrite doped with Cu and Sm (NZCSF) nanopowders were prepared by the auto-combustion method. Detailed experimental procedures for both types of materials can be found elsewhere [3,7]. Different mass ratios of the obtained powders (i.e. BT:NZCSF of 70:30, 80:20 and 90:10, corresponding to BT-NZCSF/70-30 BT-NZCSF/80-20 and BT-NZCSF/90-10 samples, respectively) were mixed and homogenized in ball mill with isopropyl alcohol as a mixing medium. After drying, the composite nanopowders were uniaxially pressed into disks of 10 mm in diameter with pressure of 196 MPa. The sintering was performed in air at 1080 °C for 4 h with a heating rate of 5 °C/ min.

X-ray diffraction measurements were carried out in order to determine formed crystal structure (Rigaku MiniFlex 600 instrument). Scanning electron microscopy (Tescan VEGA TS 5130MM) was used to analyse the microstructure of the obtained ceramics. The average grain size was determined from SEM micrographs using linear intercept technique. The density of the composite ceramics was calculated geometrically. The samples for the electrical measurements were prepared by polishing and applying gold electrodes on both sides of the samples. Ferroelectric and leakage current measurements were carried out in the electric field range of 1–38 kV/cm on a Precision Multiferroic Test System with High Voltage Interface (Radiant Technologies, Inc.). Impedance measurements of the ceramics were carried out in the temperature range 150–300 °C, with a step of 25 °C and in the frequency range 42 Hz–1 MHz using a HIOKI 3532-50 LCR HiTester. Collected data were analysed using the commercial software package ZView. Magnetic measurements of the composite materials were carried out using a superconducting quantum interferrometric magnetometer SQUID (Quantum Design).

Humidity sensitivity was analysed in a climate chamber JEIO TECH TH-KE-025, where the relative humidity (*RH*) was changed from 30–90%. Sensitivity was investigated by two point resistivity measurements due to the high resistivity of ceramic samples and DC resistivity was measured at 30 °C using a megaohmmeter MA2073 (Iskra, Kranj).

III. Results and discussion

3.1. Structural analysis

The XRD results of the composite BT-NZCSF/70-30, BT-NZCSF/80-20 and BT-NZCSF/90-10 ceramics sintered at 1080 °C for 4 h are presented in Fig. 1. The formation of barium titanate tetragonal crystal structure and nickel zinc ferrite cubic spinel structure was identified by the appearance of characteristic diffraction peaks according to JCPDS file No. 05-0626 and JCPDS file No. 10-0325, respectively. A low concentration of bar-

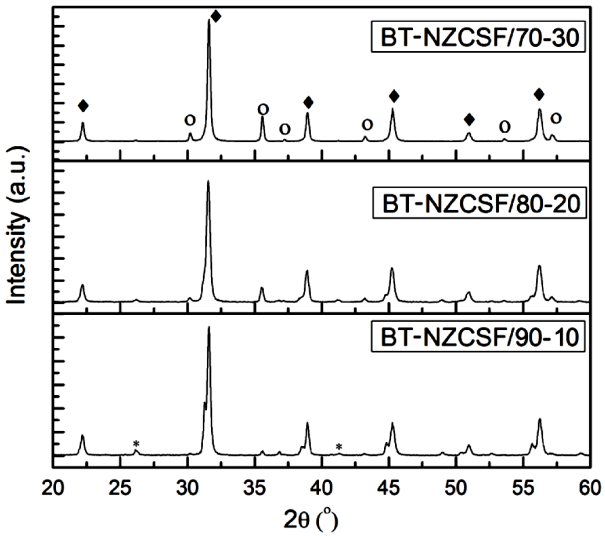

Figure 1. XRD results of the sintered BT-NZCSF/70-30, BT-NZCSF/80-20 and BT-NZCSF/90-10 ceramics (♦ - $BaTiO_3$; ○ - $NiFe_2O_4$; * - $BaCO_3$)

ium carbonate as a secondary phase can be noticed in the ceramics with higher content of barium titanate.

The intensities of characteristic peaks change according to the mass ratio between the phases. The splitting in the (002)/(200) doublet at 45° in the barium titanate phase proved the formation of the BT tetragonal phase. In the composite ceramics with higher amount of magnetic phase a distortion in the crystal lattice obviously occurred and can be correlated with magnetoelectric coupling in the composite. On the other hand, it is proven by previous research [7,18] that by slight doping of barium titanate, lattice can be deformed and tetragonal structure can change into the pseudo-cubic. The possible explanation can be also interpreted by the fact that doping with very low amount of Fe during the sintering process (that cannot be noticed from the XRD) can also affect change of BT crystal lattice and can lead toward the pseudo-cubic type of crystal symmetry.

Scanning electron microscopy was used to analyse the microstructure of the ceramic materials. The optimization of the sintering process was performed in order to avoid the formation of secondary phases in MFs, caused by the interface reaction between two phases, and the used sintering temperature was quite low for this type of ceramics. Based on previous research on pure phases, much higher sintering temperatures were needed for getting high density single phase ceramics (1300 °C for barium titanate and 1250 °C for nickel ferrite). The highest temperature at which no interface reaction occurs was found to be 1080 °C. Therefore, lower sintering temperature enabled the formation of quite porous microstructure. Even the increase of sintering time did not have significant influence on the densifi-

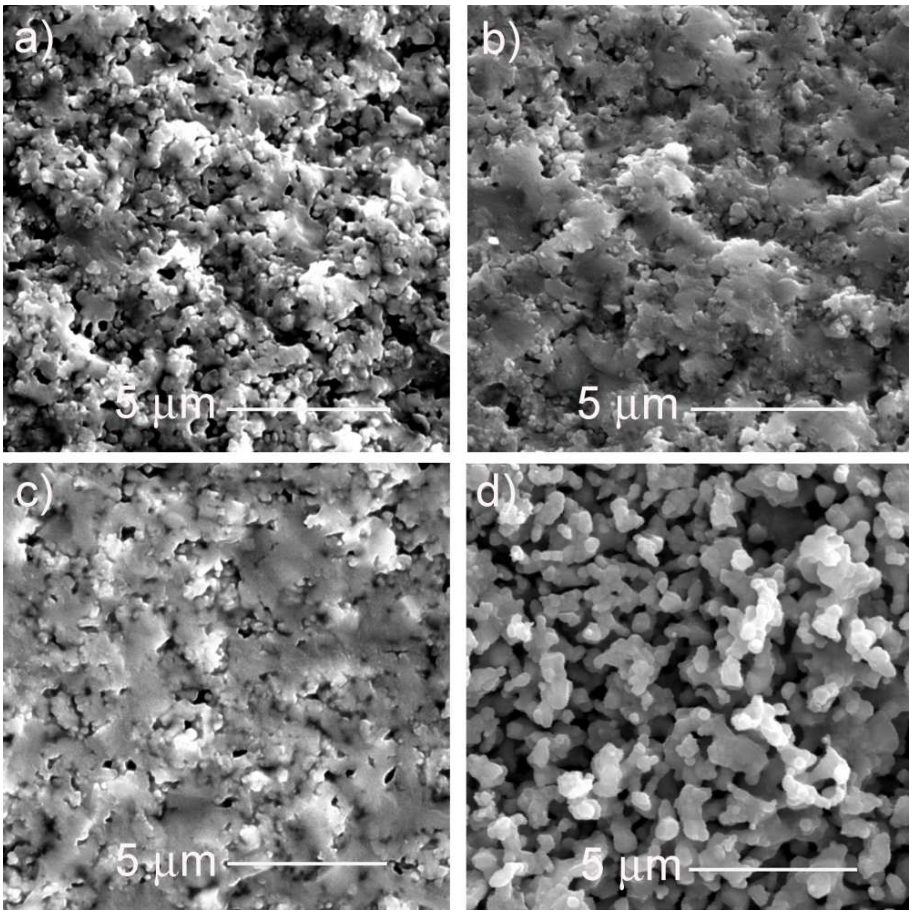

Figure 2. Microstructures of: a) BT-NZCSF/70-30, b) BT-NZCSF/80-20, c) BT-NZCSF/90-10 ceramics sintered at 1080 °C for 4 h and d) pure NZCSF sintered at 1250 °C for 4 h

cation of the composite ceramics. Prolongation of sintering time led to inhomogeneous grain growth and optimal sintering time was 4 h. Microstructures at fracture surface of the composite ceramics are presented in Fig. 2. The formation of polygonal grains can be noticed in all investigated ceramics. The density of the ceramics decreased with concentration of titanate phase, as for the BT-NZCSF/70-30, BT-NZCSF/80-20 and BT-NZCSF/90-10 they were around 89, 85 and 82% of theoretical value, respectively. As it can be seen from the Fig. 2d, the pure NZCSF ceramics, even sintered at higher temperature (1250 °C), is highly porous (it has density of only 70% of theoretical value). Thus, compatible packaging of ferrite grains with barium titanate increased the overall density of the ceramic composites.

3.2. *Ferroelectric and leakage current density measurements*

The *P-E* hysteresis loops were measured at room temperature for all investigated compounds and presented in Fig. 3. Applied electric field was in the range of 1–38 kV/cm, depending on the type of ceramics and its breakdown field. It was evidenced that all three types of compositions possessed similar electrical stability since the break down field for the BT-NZCSF/70-30 and BT-NZCSF/80-20 composites was 35 kV/cm and for BT-NZCSF/90-10 was 38 kV/cm. For the comparison, the loops measured at the same maximum electric field of 35 kV/cm were presented. Ferroelectric hysteresis loops were roundish and not typical for classical ferroelectric material (inset, pure BT) due to the high conductivity of ferrite phase in the materials. It was an evidence that in MFs, due to the existence of non-ferroelectric ferrite phase, ferroelectric properties are being deteriorated. The formation of non-saturated curves makes it difficult to determine the P_r and E_c values for the composite materials.

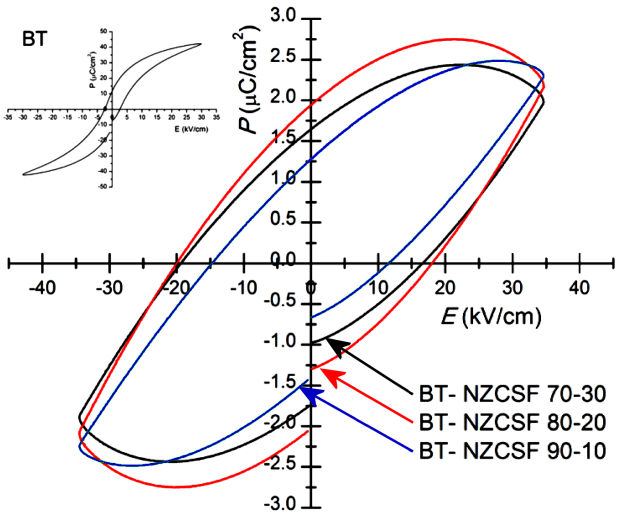

Figure 3. The *P-E* hysteresis loops at room temperature for all BT-NZCSF composites and pure $BaTiO_3$ as an inset

In order to confirm this assumption and to study the conductivity mechanism in the material, the leakage-current density (j) was measured as a function of static electric-field (E). j-E characteristics are presented on the semi-logarithmic and log-log plots in Fig. 4. As it was expected, the lowest value for leakage current density was found in the composition with the highest concentration of BT.

On the other hand, the results obtained for other two compositions did not follow the same trend. The conduction mechanism in the ceramics was analysed by plotting $\log j$ versus $\log E$ (Fig. 4b), in which nearly straight lines were noticed for the BT-NZCSF/90-10 and BT-NZCSF/70-30 composites and with two regions of different slopes for the BT-NZCSF/80-20 sample. The obtained curves were well fitted with power law: $j \sim E^m$, where m is the slope of the linear part of the curve in the log-log plots which determines the nature of conduction [23]. The values $m \neq 1$ represent deviation from the Ohm's low. For the BT-NZCSF/90-10 and BT-NZCSF/70-30 composites the m is less than 1, suggesting the grain boundary limited conduction - GBLC. In the polycrystalline dielectric material, the resistivity of the grain boundaries may be much higher

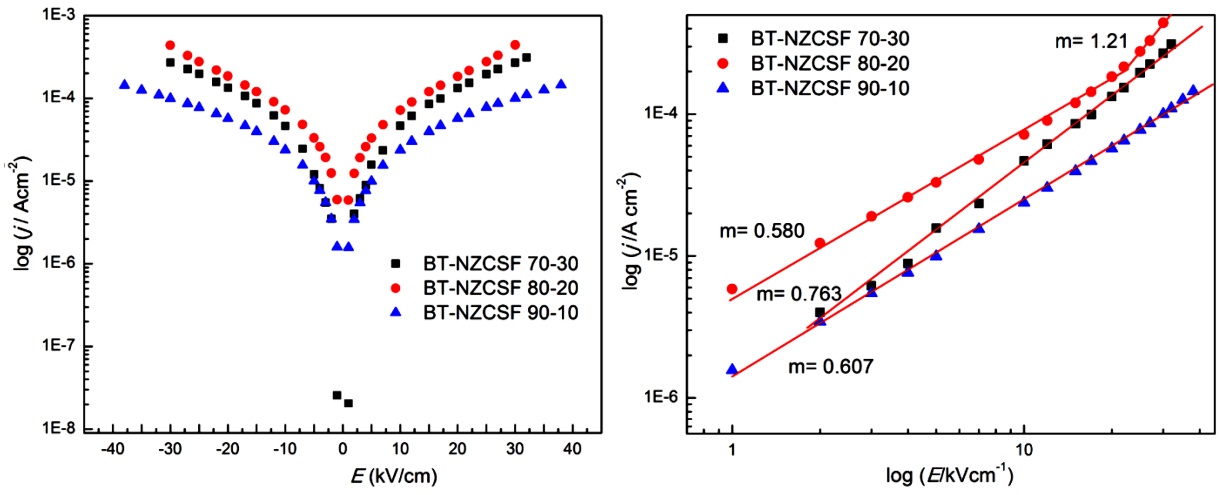

Figure 4. Leakage measurements presented in the form of: a) log$j$-E and b) log$j$-log$E$ plots

than that of the grains. Thus, the conduction current could be limited by the electrical properties of the grain boundaries [24]. In the case of the BT-NZCSF/80-20, the slop of the first region was lower than 1, indicating also GBLC mechanism and the second region with m value a bit higher than 1 which indicated the coexistence of ohmic and space charge limited conduction mechanism - SCLC. The electrical field required for the transition from GBLC to SCLC regime was found to be around 21.3 eV/cm. It is important to point out the fact that these samples are porous and the effective distance between the electrodes can vary, which can complicate the interpretation of the experimental data obtained by both electrical and ferroelectric characterization.

3.3. Impedance analysis

The impedance spectroscopy (IS) analysis was performed in the air in the temperature range of 150–300 °C with a step of 25 °C. The obtained IS results are presented in terms of impedance (Z) formalism. Variation of the imaginary part of impedance (Z'') as a function of the real part (Z') gives the complex impedance spectrum (Nyquist plots). The shapes of these plots are temperature dependent and Nyquist plots for all ceramics are presented in Fig. 5. Fitting of results was performed using software package ZView with equivalent circuits consisted of two or three parallel *R-CPE* elements connected in series. This program was used for the evaluation of the grain (R_g) and grain boundary (R_{gb}) resistivity contributions for all composite ceramics.

Total resistivity of the BT-NZCSF/70-30 composite is the lowest due to the highest concentration of conductive ferrite phase in the system. Even though it was not expected, the extracted resistivity data have shown that the BT-NZCSF/80-20 composite possessed the highest values in the whole temperature range. According to SEM analysis and measured density, the composites with 80 and 90 wt.% of BT are quite similar but there is obvious difference in the conductivity mechanisms present in these ceramics. Grain and grain boundary conductivities were calculated using the equations $\sigma_g = 1/R_g$ and $\sigma_{gb} = 1/R_{gb}$, where R_g and R_{gb} are resistivity data extracted from the impedance analysis. Temperature dependence of the grain and grain boundary conductivity followed the Arrhenius equation $\sigma = \sigma_0 \exp(-E_a/k_bT)$ and plots $\ln\sigma$ vs. $1000/T$ were presented in Fig. 6. The values of the slops represent the activation energies for the conduction processes through the grains and grain boundaries.

The activation energy necessary for electron hopping

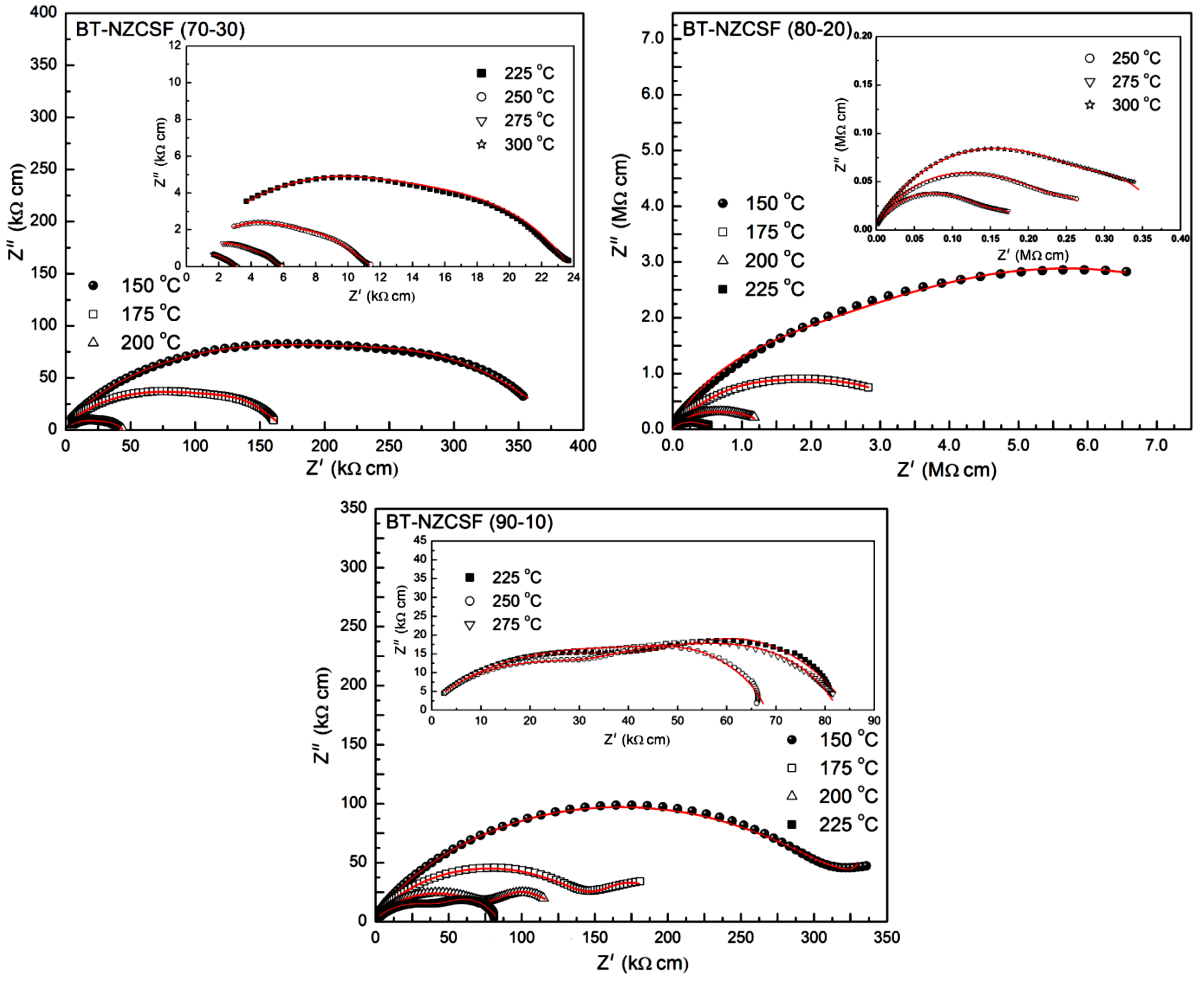

Figure 5. Complex impedance spectra of ceramics in temperature range 150–300 °C

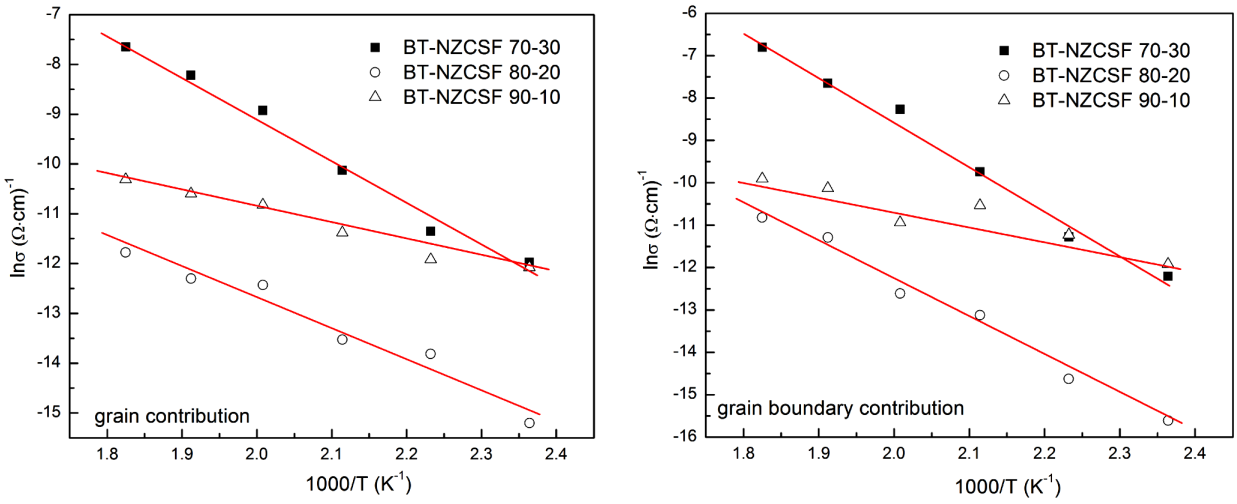

Figure 6. The Arrhenius plots of a) σ_g and b) σ_{gb} and obtained activation energies for all investigated ceramics

conduction, found in the literature, is very low, ~0.2 eV [25–27]. Usually, it is less than 0.2 eV for n-type polaronic conduction and above 0.2 eV for polaronic conduction of the holes. Previous research has shown that the activation energy value above the 0.7 eV may correspond to the mobility of the defects in the crystal lattice [27]. According to the obtained results, for all composite materials, the activation energies were approximately from 0.2 eV up to 0.6 eV which can suggest the mechanism of polaronic conduction of both types. A bit higher value of activation energy was found for grain boundaries, indicating a little stronger impact of grain boundaries on the total conductivity of the composites. The explanation can be found also in the defect chemistry. In the ferroelectrics, in ferrites and their composites, hopping conduction is favoured in ionic lattices where the same kind of cation is found in two different states [28]. In the barium titanate, hopping of 3*d* electrons from Ti^{4+} to Ti^{3+} state is possible and in nickel ferrite among Fe^{2+} to Fe^{3+}, promoting in that way the conduction of n-type in the material. The increase in Ni^{2+} ions at the B site leads to the replacement of Fe^{3+} ions at B site, leading to a decrease of ferrous ions formed. The presence of Ni^{2+}/Ni^{3+} ions and Cu^{2+}/Cu^{+}, which can give rise to p-type carriers, contributes to the net polarization. The Ni^{2+} ions limit the degree of $Fe^{2+}\leftrightarrow Fe^{3+}$ transfer, thereby obstructing electron hopping and resulting in an increase in resistivity. Since samarium also replaces iron in the lattice, it likewise hinders hopping of electrons. According to the obtained results for the activation energies, the contribution of p-type hopping conduction is obviously more dominant in the composites with more ferrite phase. On the other hand, the lowest value of activation energy was found in the BT-NZCSF/90-10 composite, indicating the dominant hopping of electrons between $Ti^{3+}\leftrightarrow Ti^{4+}$ and $Fe^{2+}\leftrightarrow Fe^{3+}$ as well.

AC conductivity (σ_{AC}) is calculated using the relation, $\sigma_{AC} = \varepsilon_0 \cdot \varepsilon'' \cdot \omega$, where ε_0 is the permittivity of the free space, the ε'' is the imaginary part of dielectric permittivity and ω is the angular frequency. Figure 7 represents logarithmic dependence of AC conductivity on angular frequency in the temperature range 20–275 °C for all three composite materials. Characteristic curves indicated the evident temperature dependence of AC conductivity. The diagrams above 150 °C in the low-frequency range have shown the tendency to form frequency independent plateau, indicating the value of DC conductivity which is attributed to the long range translational motion of the charge carriers [29]. On the other hand, in the high frequency range a dispersion region can be noticed and it can be explained by the hopping of charged particles from one localized state to another. In the high-frequency dispersion region the AC conductivity is found to obey a power low proposed by Jonscher [30] which can be presented as: $\sigma(\omega) = \sigma_0 + A(T) \cdot \omega^n$, where coefficient A and exponent n are temperature and materials intrinsic property dependent constants.

The value of exponent n can be determined from the slope of the presented plots and its value is usually between 0 and 1. Deviations from the power low correspond to n increasing with frequency and here, as in majority of disordered solids, n value in the high frequency region is between 0.5 and 1.0. Literature data [31–33] have shown that the conductivity mechanism in any material could be understood from the temperature dependent behaviour of n. To comprehend the electrical conduction mechanism in the materials, different models have been proposed (regarding frequency and temperature dependence of the exponent n). If the exponent n depends on the frequency but it is temperature independent, the quantum mechanical tunnelling (QMT) model can be proposed where the conductivity is believed to be due to the phonon-assisted tunnelling between defect states. If the exponent n is both frequency and temperature dependent, then the overlapping large-polaron tunnelling (OLPT) model can be acceptable. In this model, tunnelling of polarons is the dominant mechanism; the large polaron wells at two sites overlap and reduce the polaron-hopping energy. Finally, if the exponent n decreases with temperature, the correlated barrier hopping

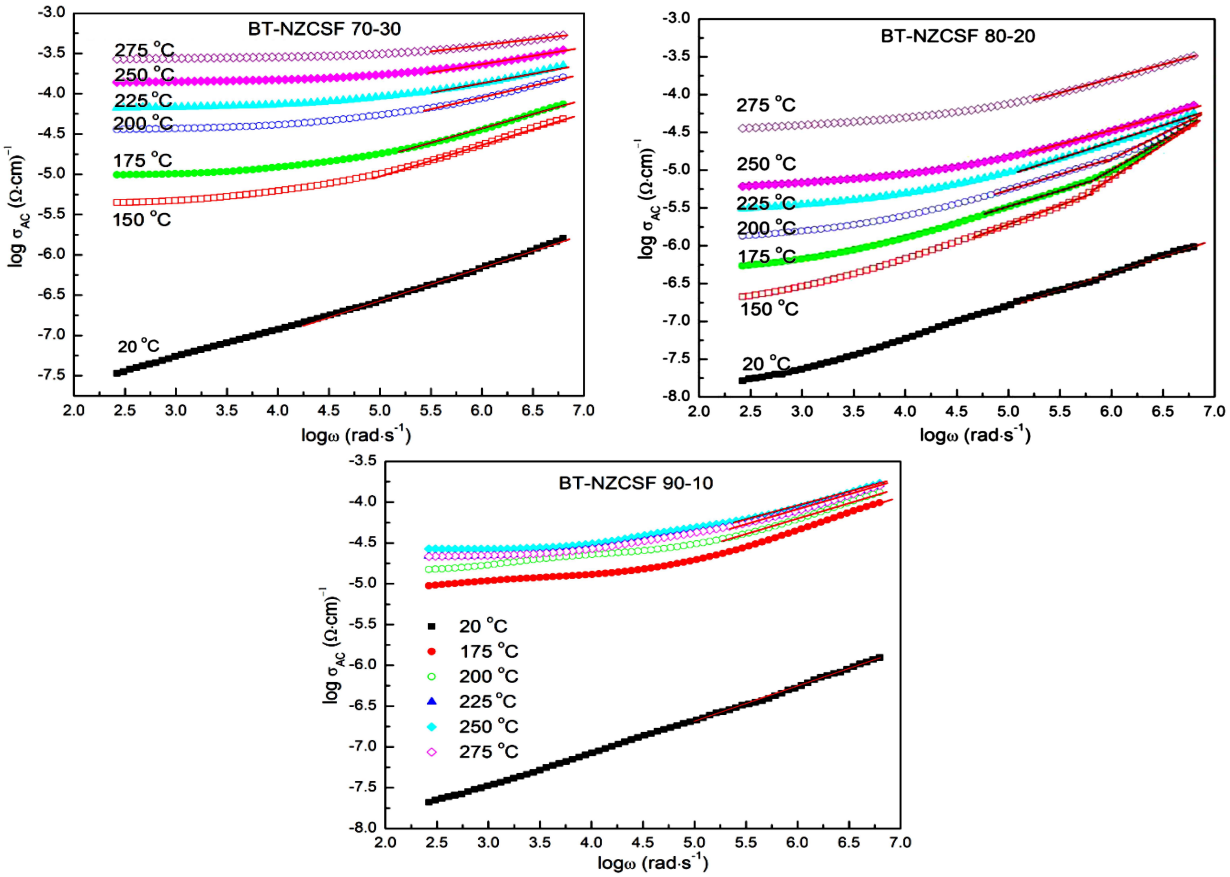

Figure 7. Variation of AC conductivity with angular frequency at temperatures between 20 and 275 °C

(CBH) model can be suggested, according to which the charge transport occurs between localized states due to the hopping over the potential barriers [32].

The behaviour of n obtained from this study differs for each composite material, indicating the influence of mass ratio between the phases in the composite. In the BT-NZCSF/70-30 composite, exponent n decreases with temperature and it is also frequency dependent, proposing the CBH model of conduction in the material. Otherwise, dispersions in the high frequency region in the temperature range 150–200 °C was observed in the BT-NZCSF/80-20 composite. The value of n (from 0.72 for lower temperatures to around 0.30 for higher) signified the coexistence of two QMT and CBH models. In the BT-NZCSF/90-10 composite the value n just slightly changes with increase of temperature (from 0.38 down to 0.30), designating the conduction mechanism to be phonon-assisted tunnelling between defect states (QMT).

3.4. Humidity sensitivity and stability

Since lot of types of ferrites as well as barium titanate are known as a good humidity sensing materials, humidity sensitivity was also analysed in this work. The humidity sensitivity of all ceramic samples was measured in the climate chamber where RH was changed from 30–90% at 30 °C. When material is placed in the humid atmosphere, the water molecules that are adsorbed on the surface can release electrons to the conduction band, resulting in the decrease of the electrical resistivity. Additionally, the presence of porosity and pore size distribution are also among the determinative factors for humidity sensors. The change of materials sensitivity (in %) is given by the equation $(R_0 - R_{(RH)})/R_0 \times 100$, where R_0 is the resistivity at the starting point of measurements (RH = 30%) and $R_{(RH)}$ is the resistivity at each RH [34], and it is shown in Fig. 8.

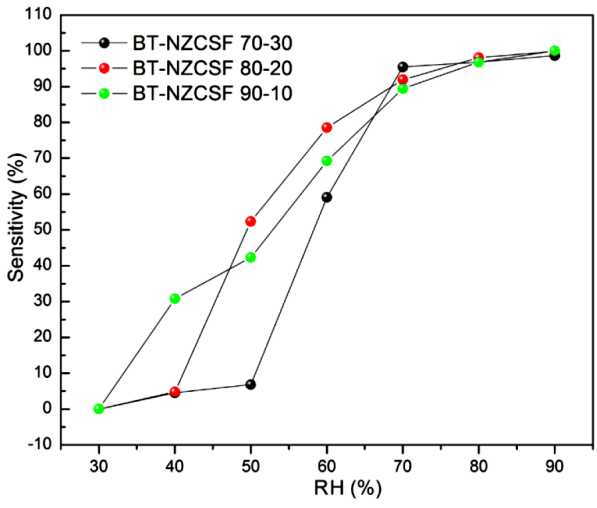

Figure 8. Sensitivity of composite materials vs. relative humidity (RH)

With increasing humidity the sensitivity of materials increases, showing the response of the material to the humid atmosphere. The fastest change was noticed in the composite with the highest concentration of barium titanate even though this material was the most dense one. When *RH* is low, water molecules chemisorb on the grain surfaces due to the formation of chemical bonds between the surface oxygen with the first water layer. Further change in humidity does not affect these bonds. Further layers of water molecules are physically adsorbed and its dissociation under the high electric field effect is possible, according to the reaction: $2\,H_2O \rightarrow H_3O^+ + OH^-$. The charge transport occurs when the hydroxyl groups as a surface charge carriers release a proton to a neighbouring water molecule, which upon receiving it releases another proton and so on [35,36]. Clearly, the concentration of the surface oxygen plays important role in the humidity sensing. Higher concentration of oxygen enables quicker response of the sensor explaining the reason why the composites with higher concentration of barium titanate developed mostly these kinds of properties.

3.5. Magnetic properties

Magnetic hysteresis loops for pure magnetic phase and all composites were presented in Fig. 9. Well saturated and narrow hysteresis loops were formed for each mixed system, evidencing the presence of ordered magnetic structure of soft ferrites.

This magnetic structure is derived from the unbalanced antiparallel spins between Fe^{3+} ions at tetrahedral sites and Ni^{2+} ions at octahedral sites [3]. As it was noticed by other authors, the addition of Cu^{2+} ions lead to the decrease of saturation magnetization in comparison with the pure NZF ceramics [7,25]. On the other hand, Sm was added in order to obtain lower values of H_c, but it was not successful in the present case. Possibly, much higher concentrations of Sm will give proper magnetic properties modification in this type of ceramics. The change in magnetic parameters in the composites was expected due to the co-existence of ferroelectric phase together with ferrite phase. When compared with the pure ferrite phase, saturation magnetization decreases. Pure ferrite phase exhibits the highest saturation of 62 emu/g and the rest of the samples demonstrate much lower values. Higher H_c values for the composites; between 63 and 84 Oe, suggested that the increase of dissipation energy was triggered by non-magnetic BT phase which could act as pores and to break the magnetic circuit [37]. Therefore, the magnetization of the composites is lower than for the pure ferrite phase and corresponds to the weight fraction of the ferrite as indicated in the name of the samples. One exception is the BT-NZCSF/90-10 composite in which the magnetization should be approximately 6 emu/g, but it is significantly lower, i.e. only 2 emu/g. Perhaps the true weight fraction is lower than the nominal composition suggests. Remnant magnetization decreases with BT concentration but for the BT-NZCSF/70-30 ceramics it possesses the same value as for the pure ferrite phase. Clearly, the interface effects slightly affect magnetic interactions and they are just proportional to the amount of ferrite phase in the composite.

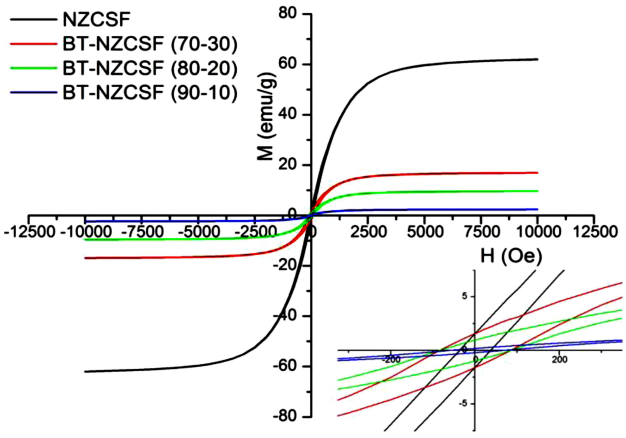

Figure 9. Magnetic hysteresis loops $M(H)$ obtained for all composites and pure NZCSF

IV. Conclusions

Composites containing spinel nickel-zinc ferrite doped with copper and samarium and ferroelectric barium titanate were prepared by mixing method. Sintering conditions were selected from the detailed optimization process and all ceramics were sintered at 1080 °C for 4 h. Roundish ferroelectric hysteresis loops have shown deterioration of ferroelectric properties due to the existence of non-ferroelectric and very conductive ferrite phase. Different kinds of conductivity mechanisms in the composite materials were detected from the measurement of the leakage-current density as a function of static electric-field. For the composites with 10 and 30 wt.% of ferrite phase the grain boundary limited conduction - GBLC was suggested. In the case of the composites with 20 wt.% of ferrite phase there were two regions of interest, the first region indicated also GBLC mechanism while the second region indicated the coexistence of ohmic and space charge limited conduction mechanism - SCLC. The impedance analysis suggested a bit stronger impact of grain boundaries on the total conductivity of the composites and the mechanism of polaronic conduction of two types. Detailed explanations were given through the defect chemistry based on hopping of 3*d* electrons in the system. The highest humidity sensitivity was noticed in the composite with the highest concentration of barium titanate suggesting the main influence of ferroelectric phase on the humidity sensing properties.

Magnetic measurements have shown that the interface effects slightly affect magnetic interactions and they are just proportional to the amount of ferrite phase in the composite. The soft magnetic nature of these

composites might be very useful for multifunctional devices which can switch the magnetization with small external magnetic field.

Acknowledgments: The authors gratefully acknowledge the Ministry of Education, Science and Technological Development of Republic of Serbia for the financial support of this work (projects 451-03-68/2020-14/200053 and 451-03-68/2020-14/200134). Special thanks to Dr. Sašo Gyergyek from the Jožef Stefan Institute, Ljubljana, Slovenia, for magnetic measurements.

References

1. L. Mitoseriu, V. Buscaglia, M. Viviani, M.T. Buscaglia, I. Pallecchi, C. Harnagea, A. Testino, V. Trefiletti, P. Nanni, A.S. Siri, "$BaTiO_3$-$Ni_{0.5}Zn_{0.5}Fe_2O_4$ ceramic composites with ferroelectric and magnetic properties", *J. Eur. Ceram. Soc.*, **27** (2007) 4379–4382.
2. H. Palneedi, V. Annapureddy, S. Priya, J. Ryu, "Status and perspectives of multiferroic magnetoelectric composite materials and application", *Actuators*, **5** (2016) 9.
3. R. Grigalaitis, M.M. Vijatović Petrović, J.D. Bobić, A. Dzunuzovic, R. Sobiestianskas, A. Brilingas, B.D. Stojanović, J. Banys, "Dielectric and magnetic properties of $BaTiO_3$-$NiFe_2O_4$ multiferroic composites", *Ceram. Int.*, **40** (2013) 6165–6170.
4. R.J. Pandya, U.S. Joshi, O.F. Caltun, "Microstructural and electrical properties of barium strontium titanate and nickel zinc ferrite composites", *Procedia Mater. Sci.*, **10** (2015) 168–175.
5. R. Samad, M.D. Rather, K. Asokan, B. Want, "Magneto-dielectric studies on multiferroic composites of Pr doped $CoFe_2O_4$ and Yb doped $PbZrTiO_3$", *J. Alloys Compd.*, **744** (2018) 453–462.
6. A. Jain, A.K. Panwar, A.K. Jha, Y. Sharma, "Improvement in dielectric, ferroelectric and ferromagnetic characteristics of $Ba_{0.9}Sr_{0.1}Zr_{0.1}Ti_{0.9}O_3$-$NiFe_2O_4$ composites", *Ceram. Int.*, **43** (2017) 10253–10262.
7. A. Dzunuzovic, M. Vijatovic Petrovic, B. Stojadinovic, N. Ilic, J. Bobic, C. Foschini, M. Zaghete, B. Stojanovic, "Multiferroic (NiZn)Fe_2O_4-$BaTiO_3$ composites prepared from nanopowders by auto-combustion method", *Ceram. Int.*, **41** (2015) 13189–13200.
8. R. Mondal, B. Murty, V. Murthy, "Dielectric, magnetic and enhanced magnetoelectric response in high energy ball milling assisted BST-NZF particulate composite", *Mater. Chem. Phys.*, **167** (2015) 338–346.
9. R.S. Devan, B.K. Chougule, "Magnetic properties and dielectric behavior in ferrite/ferroelectric particulate composites", *Physica B*, **393** (2007) 161–166.
10. S.A. Lokare, D.R. Patil, R.S. Devan, S.S. Chougule, Y.D. Kolekar, B.K. Chougule, "Electrical conduction, dielectric behavior and magnetic effect in $x$$BaTiO_3$ + (1-x)$Ni_{0.94}Co_{0.01}Mn_{0.05}Fe_2O_4$ ME composites", *Mater. Res. Bull.*, **43** (2008) 326–332.
11. G. Ravi Kumar, K. Vijaya Kumar, Y. Chetty Venudhar, "Synthesis, structural and magnetic properties of copper substituted nickel ferrites by sol-gel method", *Mater. Sci. Appl.*, **3** (2012) 87–91.
12. V.J. Pissurlekar, "Magnetic and structural properties of $NiZnFe_2O_4$ ferrite nanopowders doped with Cu^{2+}", *Int. J Sci. Res.*, **5** (2016) 1147–1149.
13. K. Mujasam Batoo, M. Shahnawaze Ansari, "Low temperature-fired Ni-Cu-Zn ferrite nanoparticles through auto-combustion method for multilayer chip inductor applications", *Nanoscale Res. Lett.*, **7** (2012) 112.
14. B. Suryanarayana, K. Chandra Mouli, V. Raghavendra, B.B. Parvateesam, "Synthesis and magnetic studies of Ni-Cu-Zn ferrite nanocrystals", *Indian J. Res. Pharm. Biotech.*, **1** (2014) 92–94.
15. L. Gama, A.P. Diniz, A.C.F.M. Costa, S.M. Rezende, A. Azevedo, D.R. Cornejo, "Magnetic properties of nanocrystalline Ni-Zn ferrites doped with samarium", *Physica B*, **384** (2006) 97–99.
16. M. Ušáková, E. Ušák, M. Šoka, "Study of magnetic properties of samarium substituted nickel-zinc ferrites", *J. Electr. Eng.*, **66** (2015) 112–115.
17. J. Shah, R.K. Kotnala, B. Singh, H. Kishan, "Microstructure-dependent humidity sensitivity of porous $MgFe_2O_4$-CeO_2 ceramic", *Sensors Actuators B*, **128** (2007) 306–311.
18. M.M. Vijatovic Petrovic, A. Radojkovic, J.D. Bobic, A. Dzunuzovic, N. Ilic, B.D. Stojanovic, "Sensing properties of barium titanate nanoceramics tailored by doping and microstructure control", *J. Mater. Sci.*, **54** (2019) 6038–6052.
19. J. Wang, X. Wang, X. Wang, "Study on dielectric properties of humidity sensing nanometer materials", *Sensors Actuators B*, **108** (2005) 445–449.
20. H. Farahani, R. Wagiran, M. Nizar Hamidon, "Humidity sensors principle, mechanism, and fabrication technologies: a comprehensive review", *Sensors*, **14** (2014) 7881–7939.
21. Z. Chen, C. Lu, "Humidity sensors: A review of materials and methods", *Sensor Lett.*, **3** (2005) 274–295.
22. M. Viviani, M.T. Buscaglia, V. Buscaglia, M. Leoni, P. Nanni, "Barium perovskites as humidity sensing materials", *J. Eur. Ceram. Soc.*, **21** (2001) 1981–1984.
23. S. Godara, B. Kumar, "Effect of Ba-Nb co-doping on the structural, dielectric, magnetic and ferroelectric properties of $BiFeO_3$ nanoparticles", *Ceram. Int.*, **41** (2015) 6912–6919.
24. F.C. Chiu, "A review on conduction mechanisms in dielectric films", *Adv. Mater. Sci. Eng.*, **2014** (2014) 578168.
25. A.S. Dzunuzovic, M.M. Vijatovic Petrovic, J.D. Bobic, N.I. Ilic, M. Ivanov, R. Grigalaitis, J. Banys, B.D. Stojanovic, "Magneto-electric properties of x$Ni_{0.7}Zn_{0.3}Fe_2O_4$ – (1-x)$BaTiO_3$ multiferroic composites", *Ceram. Int.*, **44** [1] (2018) 683–694.
26. V.V. Awati, "Synthesis and characterization of Ni-Cu-Zn ferrite materials by auto combustion technique", *Int. J. Chem. Phys. Sci.*, **4** (2015) 50–59.
27. M.M. Vijatovic Petrovic, R. Grigalaitis, A. Dzunuzovic, J.D. Bobic, B.D. Stojanovic, R. Salasevicius, J. Banys, "Positive influence of Sb doping on properties of di-phase multiferroics based on barium titanate and nickel ferrite", *J. Alloys Compd.*, **749** (2018) 1043–1053.
28. C.E. Ciomaga, A.M. Neagu, M.V. Pop, M. Airimioaei, S. Tascu, G. Schileo, C. Galassi, L. Mitoseriu, "Ferroelectric and dielectric properties of ferriteferroelectric ceramic composites", *J. Appl. Phys.*, **113** (2013) 074103.
29. R. Das, R.N.P. Choudhary, "Structure, dielectric and electrical properties of relaxor lead-free double perovskite: Nd_2NiMnO_6", *Process. Appl. Ceram.*, **13** [1] (2019) 1–11.
30. S. Kumar, K.B.R. Varma, "Dielectric relaxation in bis-

muth layer-structured $BaBi_4Ti_4O_{15}$ ferroelectric ceramics", *Curr. Appl. Phys.*, **11** (2011) 203–210.
31. B.M. Greenhoe, M.K. Hassan, J.S. Wiggins, K.A. Mauritz, "Universal power law behavior of the AC conductivity versus frequency of agglomerate morphologies in conductive carbon nanotube-reinforced epoxy networks", *J. Polym. Sci. B Pol. Phys.*, **54** (2016) 1918–1923.
32. V. Thakur, A. Singh, A.M. Awasthi, L. Singh, "Temperature dependent electrical transport characteristics of $BaTiO_3$ modified lithium borate glasses", *AIP Advances*, **5** (2015) 087110.
33. A.K. Roy, A. Singh, K. Kumari, K. Amar Nath, A. Prasad, K. Prasad, "Electrical properties and AC conductivity of $(Bi_{0.5}Na_{0.5})_{0.94}Ba_{0.06}TiO_3$ ceramic", *ISRN Ceramics*, **2012** (2012) 854831.
34. C.L. Cao, C.G. Hu, L. Fang, S.X. Wang, Y.S. Tian, C.Y. Pan, "Humidity sensor based on multi-walled carbon nanotube thin films", *J. Nanomater.*, **2011** (2011) 707303.
35. H. Farahani, R. Wagiran, M. Nizar Hamidon, "Humidity sensors principle, mechanism, and fabrication technologies: a comprehensive review", *Sensors*, **14** (2014) 7881–7939.
36. Z. Chen, C. Lu, "Humidity sensors: A review of materials and methods", *Sensor Lett.*, **3** (2005) 274–295.
37. N. Adhlakha, K.L. Yadav, "Study of structural, dielectric and magnetic behavior of $Ni_{0.75}Zn_{0.25}Fe_2O_4$-$Ba(Ti_{0.85}Zr_{0.15})O_3$ composites", *Smart Mater. Struct.*, **21** (2012) 115021.